J. Phase Equilib. Diffus. (2020) 41:103–115
https://doi.org/10.1007/s11669-020-00785-6

Coupled Experimental Study and Thermodynamic Modeling of the MgO-MnO-Mn_2O_3-Ti_2O_3-TiO_2 System

Sourav Kumar Panda[1] · **In-Ho Jung**[2]

Submitted: 18 January 2020 / in revised form: 30 January 2020 / Published online: 24 February 2020

Abstract A coupled phase diagram experiment and thermodynamic modeling of the MgO-MnO-Mn_2O_3-Ti_2O_3-TiO_2 system at 1 bar total pressure is presented. High temperature equilibration and quenching experiments followed by the phase analysis using electron probe microanalysis and X-ray diffraction were performed to obtain complex phase equilibria between solid solutions and liquid phase in air. Low temperature phases during quenching was inevitable in some samples which lead to inaccuracy in the experimental data. The molten oxide phase was described by using the Modified Quasichemical Model, which considers short-range ordering in liquid state, and the Gibbs energies of the extensive solid solutions (pseudobrookite, ilmenite and spinel) were described using the Compound Energy Formalism based on their crystal structures. A set of optimized model parameters of all phases was obtained, which reproduces all the reliable experimental data within experimental error limits from 25 °C to above the liquidus temperatures over the entire range of composition at air atmosphere. The model can also predict the phase equilibria in the range of oxygen partial pressures from metallic saturation to air. The complex phase relationships in the system have been elucidated for the first time and the database of the model parameters can be used with FactSage software to calculate any phase diagrams and thermodynamic properties of the MgO-MnO-Mn_2O_3-Ti_2O_3-TiO_2 system.

Keywords ilmenite · MgO–MnO–Mn_2O_3–TiO_2–Ti_2O_3 · pseudobrookite · spinel · thermodynamic modeling

1 Introduction

The MgO-MnO-Mn_2O_3-TiO_2-Ti_2O_3 system is significant for the ceramics in electronic and communication industries. The rapid development of modern microwave communication technology demands new ceramic components for electronic oscillators, filters and antenna application having low permittivity ($\varepsilon_r < 15$) which minimizes cross-coupling with conductors and decreases electronic signal transition.[1–6] These ceramics should also have extremely high-quality factor to increase selectivity and a near-zero temperature coefficient for frequency stability (low τ_f). For these purposes, recently, spinel-type (AB_2O_4 and A_2BO_4) ceramics[2,4,7] and ilmenite-type (ABO_3)[5,6,8] ceramics have attracted much scientific attention. In this regard, a good knowledge of the thermodynamic stability and the structural information (cation distribution) of extensive spinel (Mg_2TiO_4-$MgTi_2O_4$-Mn_2TiO_4-$MnTi_2O_4$-$MgMn_2O_4$-Mn_3O_4) and ilmenite ($MgTiO_3$-$MnTiO_3$-Ti_2O_3) solid solution within the Mg-Mn-Ti-O system can be very important.

In the recent years, new grade of high strength steel has been engineered by formation of an acicular ferrite type microstructure. In this steel grade, the oxide inclusions within the MgO-MnO-Mn_2O_3-TiO_2-Ti_2O_3 system are

✉ Sourav Kumar Panda
sourav.panda@tatasteeleurope.com

In-Ho Jung
in-ho.jung@snu.ac.kr

[1] Department of Mining and Materials Engineering, McGill University, 3610 University Street, Montreal, QC H3A 0C5, Canada

[2] Department of Materials Science and Engineering, and Research Institute of Advanced, Materials (RIAM), Seoul National University, 1 Gwanak-ro, Gwanak-gu, Seoul 08826, South Korea

intentionally controlled to induce such microstructure. This technology is in general termed as "oxide metallurgy". For the inclusion engineering[9–14] within the MgO-MnO-Mn_2O_3-TiO_2-Ti_2O_3 system, the accurate thermodynamic database for the Mg-Mn-Ti-O system is necessary.

However, the phase equilibria in the MgO-MnO-Mn_2O_3-TiO_2-Ti_2O_3 system are very complex due to the multiple oxidation states of Mn and Ti, and the existence of extensive solid solutions. The goal of the present study is a complete description of phase diagrams within the Mg-Mn-Ti-O system. For this purpose, all the experimental phase diagram data for the MgO-MnO-Mn_2O_3-TiO_2-Ti_2O_3 system at 1 atm total pressure with oxygen partial pressures from metallic saturation to 1 atm were critically evaluated and optimized to obtain the models with a set of model parameters to reproduce all reliable experimental data in the system. New key phase diagram experiments were also performed using the classical quenching technique to provide missing phase diagram data in air atmosphere. All the thermodynamic calculations of the present study were performed using the FactSage thermochemical software.[15] This is part of a wide research project to extend the oxide database toward high Mn and Ti oxide region.

2 Previous Works

In this study, the quaternary Mg-Mn-Ti-O system is mainly investigated. The phase diagram, thermodynamic property, and structural data in solid solution for the sub ternary oxide systems such as Mg-Mn-O,[16] Mg-Ti-O[17] and Mn-Ti-O[18] have been critically evaluated and optimized for the development of thermodynamic database. The optimization results are used directly for this study without any further modification, and therefore these sub systems will not be discussed in this study.

The phase equilibria in the quaternary Mg-Mn-Ti-O system were reviewed and investigated only by Demin et al.[19] They studied the isothermal phase equilibrium relationships for this system using classical quenching method at 1100 and 1200 °C in air $\left(p_{O_2} = 0.21\text{atm}\right)$. The equilibration was done for 200 h at 1100 °C, and 100 h at 1200 °C, respectively, followed by XRD phase analysis. Demin et al.[19] reported the presence of tetragonal spinel phase at 1200 °C in the Mn-rich region. However, according to the critical assessments of the Mg-Mn-O[16] and Mn-Ti-O[18] systems by the present authors, no tetragonal spinel phase can form at 1200 °C. We can assume that the tetragonal spinel phase in this Mg-Mn-Ti-O system by Demin et al. resulted from the transition from stable cubic spinel solution due to slow quenching process in their experiments. In the present study, therefore, the formation of tetragonal spinel at 1200 °C was not considered. Phase equilibria of this system in the oxidized atmosphere are still less known. No literature on equilibrium experiments at reduced atmosphere was found.

3 Experimental Procedure

The phase diagram study by Demin et al.[19] was only focused on the relationship at 1100 and 1200 °C and less accurate in certain region (Mn-rich region at 1200 °C). As these experimental data are insufficient to reveal the phase equilibria in the entire Mg-Mn-Ti-O system even in air atmosphere, new phase diagram experiments were conducted in this study to help the thermodynamic modeling of this system. The phase equilibria from sub-solidus temperature to liquidus temperature were determined using classical equilibration and quenching method.

First, preliminary phase diagram calculations for the Mg-Mn-Ti-O system were performed using the optimized model parameters of the constituent ternary system, Mg-Mn-O,[16] Mg-Ti-O[17] and Mn-Ti-O[18] Experimental phase diagram study in air were designed to verify the preliminary thermodynamic calculation results. In order to obtain maximum phase diagram information with minimum number of the experimental trials, key experimental compositions to produce three-phase or two-phase assemblage were intentionally selected from the preliminary calculations. If possible, one of phases was also intentionally targeted for liquid phase in order to accelerate the phase equilibrations. Multicomponent phase diagram experiments at reducing condition is more complex because the partial pressure is preciously controlled or metallic phase should be added (or metallic crucible should be used). However, we have experience that the phase diagrams at reducing atmosphere (metal saturation or low p_{O_2}) can be generally well predicted from the thermodynamic models with optimized parameters for the sub-binary and ternary systems.[20–23]

The detail description of preparation of starting materials, equilibration method, phase identification and composition analysis can be found elsewhere.[18] Raw data were reduced with the ZAF correction using periclase (Mg), garnet (Mn) and rutile (Ti) standards. The EPMA provides information only on the metal content in a phase and does not distinguish between multivalent cations. In this study, manganese was assumed to be present as Mn^{2+} and Mn^{3+} in air, while, all titanium was assumed in quadrivalent state (Ti^{4+}).[24]

4 Equilibrium Phases and Thermodynamic Models

Figure 1 shows the intermediate solid solutions in the MgO-MnO-Mn_2O_3-TiO_2-Ti_2O_3 system at 1 atm. Table 1 lists all the equilibrium phases which are observed in this system. The optimized model parameters for each phase are listed in Table 2.

4.1 Liquid Oxide Phase (Molten Slag)

The Modified Quasichemical Model (MQM),[25–28] which considers short-range ordering of second-nearest-neighbor cations in the oxide melt, was used for describing the MgO-MnO-Mn_2O_3-Ti_2O_3-TiO_2 molten slag. In the present study, the interactions between the cations such as Mg^{2+}, Mn^{2+}, Mn^{3+}, Ti^{3+}, and Ti^{4+} were considered in the MQM with O^{2-} as a common anion. That is, MnO, $MnO_{1.5}$, $TiO_{1.5}$, and TiO_2 were considered as the components in liquid slag. The components are written as $MnO_{1.5}$ and $TiO_{1.5}$ rather than Mn_2O_3 and Ti_2O_3 simply to emphasize that Mn^{3+} and Ti^{3+} ions are distributed as independent particles in the liquid slag not as ion pairs. The brief description of the MQM is given elsewhere.[16–18]

Optimized parameters for the binary and ternary subsystems within Mg-Mn-Ti-O (MgO-MnO-Mn_2O_3-Ti_2O_3-TiO_2) slag solution was obtained previously.[16–18,22] The second-nearest-neighbor 'coordination numbers' of Mg^{2+}, Mn^{2+}, Mn^{3+}, Ti^{3+} and Ti^{4+} used in the present study are the same as the previous studies.[16–18,22] In other words, the coordination number of Mn^{3+} and Ti^{3+} are identical to each other, which is $^3/_2$ of Mg^{2+} and Mn^{2+}; and $^3/_4$ times of Ti^{4+}. Once binary interactions for all the binary system are known and well determined, then parameters can be used to predict the Gibbs energy of ternary system. In the MQM, different geometric interpolation technique can be used to predict the Gibbs energy of the ternary liquid systems from the binary model parameters. The details of the interpolation technique are explained elsewhere.[29] A Kohler-like "symmetric approximation"[29] was used for all 10 ternary systems within MgO-MnO-$MnO_{1.5}$-TiO_2-$TiO_{1.5}$ system. When the predicted Gibbs energy with interpolation technique is not accurate enough to reproduce the phase equilibria in ternary higher order systems, additional ternary excess parameters can be employed. No ternary model parameters are used in 10 ternary systems except the MgO–MnO–TiO_2 system, which shows a remarkable predictive ability of MQM from the binary parameters. To reproduce the liquidus measured from the current experiments, two ternary model parameters was used for MgO-MnO-TiO_2 system (will be discussed later).

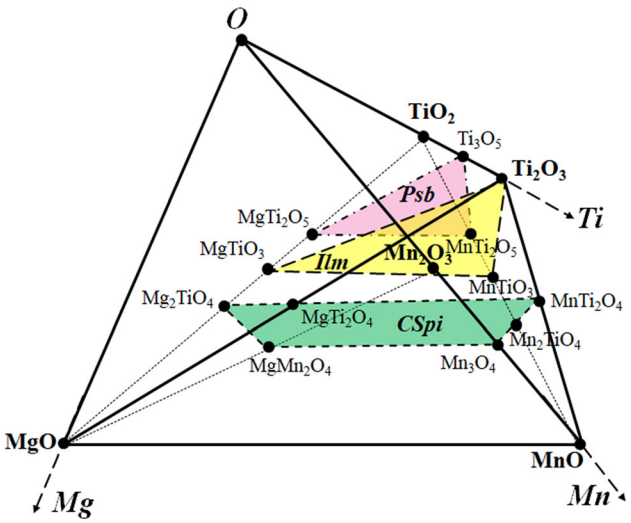

Fig. 1 Schematic diagram of the solid solution phases in the MgO-MnO-Mn_2O_3-TiO_2-Ti_2O_3 system

4.2 Pseudobrookite Solid Solution

The pseudobrookite compounds generally have an orthorhombic structure and belong to the *Cmcm* space group.[30] The solid solution has the general formula AB_2O_5, where all the A and B cations are distributed in two non-equivalent octahedrally coordinated cation sites, the *4c* (or M1 or A) sites and the *8f* (or M2 or B) sites, producing AO_6 and BO_6 octahedra, respectively.[31,32] Well known pseudobrookites are Fe_2TiO_5 (pseudobrookite), $FeTi_2O_5$ (ferropseudobrookite), $MgTi_2O_5$ (karrooite), $MnTi_2O_5$, Al_2TiO_5, $(Mg,Fe)Ti_2O_5$ (armalcolite), Ti_3O_5, etc. In fully ordered pseudobrookite, all the A cations reside in the *4c* sites while all the B cations reside in the *8f* sites. In fully disordered pseudobrookite, the composition of both *4c* and *8f* site are $(A_{0.33}B_{0.67})$. This structural information was properly implemented in the development of the present thermodynamic models for the pseudobrookite solid solution in the Mg-Mn-Ti-O system.

A two-sublattice pseudobrookite model[18] in the framework of the Compound Energy Formalism (CEF) (Hillert et al.[33]) was developed in the present study to describe the Gibbs energy of pseudobrookite solution in the Mg-Mn-Ti-O system.

The Gibbs energy of these cation site exchange reactions between the M1 and M2 sites are the model parameters; they are denoted by Δ and I parameters and described elsewhere.[18,21] The Gibbs energies of sixteen endmember are required for the model. Sixteen end-member Gibbs energies are required for the model. Among them, the Gibbs energies of four end-members (G_{GG}, G_{TT}, G_{GT}, and G_{TG}) were previously fixed in the Ti-O system,[23] five end-members Gibbs energies (G_{MM}, G_{MG}, G_{MT}, G_{GM}, and G_{TM}) were already fixed from Mg-Ti-O system,[20] and five end-

Table 1 Stable intermediate solid solutions observed in the Mg–Mn-Ti–O system

Phases(a)	Structure(b)	Space groups	Model(c)
Pseudobrookite (Psb)	$(Mg^{2+}, Mn^{2+}, Ti^{3+}, Ti^{4+})^{4c}$ $[Mg^{2+}, Mn^{2+}, Ti^{3+}, Ti^{4+}]_2^{8f}$ O_5	*Cmcm*	CEF
Ilmenite (Ilm)	$(Mg^{2+}, Mn^{2+}, Ti^{3+})^{A}$ $[Fe^{3+}, Ti^{3+}, Ti^{4+}]_2^{B}$ O_3	$R\bar{3}$	CEF
Cubic Spinel (CSpi)	$(Mg^{2+}, Mn^{2+})^{T}$ $[Mg^{2+}, Mn^{2+}, Mn^{3+}, Mn^{4+}, Ti^{3+}, Ti^{4+}, Va]_2^{O}$ O_4	$Fd\bar{3}m$	CEF
Tetragonal Spinel (TSpi)	$(Mg^{2+}, Mn^{2+}, Mn^{3+})^{T}$ $[Mg^{2+}, Mn^{2+}, Mn^{3+}, Ti^{4+}, Va]_2^{O}$ O_4	$I4_1/amd$	CEF
Monoxide (Mono)	MgO-MnO-$MnO_{1.5}$-TiO_2	$Fm\bar{3}m$	BWRM
Rutile (Rut)	TiO_2-$TiO_{1.5}$-MnO	$P4_2/mnm$	BWRM
Liquid (Liq)	MgO-MnO-$MnO_{1.5}$-TiO_2-$TiO_{1.5}$		MQM

(a) The name in parenthesis is abbreviation used in this study. (b) Cations shown within a set of brackets for the solid solutions occupy the same sublattice, and Va represents vacancy. (c) CEF: Compound Energy Formalism[33]; BWRM: Braggs William Random Mixing Model[29]; MQM: Modified Quasichemical Model[25–28]

Table 2 Optimized model parameters in the MgO-MnO-Mn_2O_3-TiO_2-Ti_2O_3 system [J/mol and J·(mol·K)$^{-1}$]

Liquid solution (Liq)(a): MgO-MnO–$MnO_{1.5}$–TiO_2–$TiO_{1.5}$

$q^{001}_{MgO,TiO_2(MnO)} = -62760$ $q^{011}_{MgO,TiO_2(MnO)} = 117152$

Pseudobrookite solid solution (Psb)(b): $MgTi_2O_5$-$MnTi_2O_5$–Ti_3O_5

$\Delta_{JMT}=(G_{JM} + G_{MT}) - (G_{MM} + G_{JT}) = 33472$ $\Delta_{MJT}=(G_{MJ} + G_{JT}) - (G_{JJ} + G_{MT}) = 0$

Ilmenite solid solution (Ilm)(b): $MgTiO_3$-$MnTiO_3$-Ti_2O_3

$L_{MJ:T} = -2092$ $L_{MJ:G} = -2092$

Cubic spinel solid solution (CSpi)(b): Mn_3O_4-Mn_2TiO_4-$MnTi_2O_4$-Mg_2TiO_4-$MgTi_2O_4$-$MgMn_2O_4$

$L_{JT:M} = -146440$ $L_{JG:M} = -146440$ $L_{MJ:T} = -20920$ $L_{MJ:G} = -20920$

Tetragonal spinel solid solution (TSpi)(b): Mn_3O_4-Mn_2TiO_4-Mg_2TiO_4-$MgMn_2O_4$

$L_{JT:M} = 33472$

The name in parenthesis is abbreviation used in this study, and, the notation M, J, K, L, G, T means Mg^{2+}, Mn^{2+}, Mn^{3+}, Mn^{4+}, Ti^{3+}, Ti^{4+}, respectively

(a) The Gibbs energies of pure solid and liquid MgO, MnO, $TiO_{1.5}$, and TiO_2 were taken from Eriksson and Pelton,[43,44] and those of solid Mn_2O_3 and pure liquid $MnO_{1.5}$ (= 0.5 Mn_2O_3) were taken from Kang and Jung.[40] The notation for the ternary parameters can be found elsewhere[29]. (b) The Gibbs energy of pseudobrookite endmembers in the Ti-O, Mn-Ti-O and Mg-Mn-O were taken from Panda and Jung,[19,21,23] and those of Mg-Ti-O system were taken from Du and Jung[20]

members Gibbs energies (G_{JJ}, G_{JG}, G_{JT}, G_{GJ}, and G_{TJ}) were already fixed from Mn-Ti-O system.[19] The Gibbs energies of the remaining two end-members (G_{MJ}, G_{JM}) were obtained in the present study using the site exchange reaction model parameters (Δ) as shown in Table 2). Very small value of model parameter was used in the present study (Δ_{JMT}) to fix the solubility of the pseudobrookite solid solution measured from the present experiments. In the present study, no excess Gibbs energy parameter was required.

4.3 Ilmenite Solution

The ilmenite compound has a trigonal (distorted hexagonal) structure and belongs to the $R\bar{3}$ space group.[34–37] The solid solution within ilmenite compounds has a general formula of XYO_3, where all the cations (X and Y) are distributed in two non-equivalent octahedrally coordinated cation sites (A and B) occupying 2/3 of the interstices. At high temperature (above the critical ordering temperature, T_c) cations get randomly distributed within A and B cation sites and the space group symmetry change from $R\bar{3}$ to $R\bar{3}c$.[38,39] The order–disorder transition for general ilmenite solution are still not well known, therefore, the transition to disordered structure was not considered in this study. Similar to pseudobrookite solid solutions, the Gibbs energy of the ilmenite solution is expressed using the CEF explained elsewhere.[18] The Gibbs energies of six end-members are required for the model. All these Gibbs energies were fixed previously: G_{GG}, G_{GT}, G_{JG}, and G_{JT} from the Ti-O and Mn-Ti-O system,[18] G_{MG} and G_{MT} from the Mg-Ti-O system.[17] Therefore, the Gibbs energy of the ilmenite solution in the Mg-Mn-Ti-O system was predicted from the end-member Gibbs energies determined in the previous Ti-O,[18] Mn-Ti-O[18] and Mg-Ti-O[17] system with a very small excess Gibbs energy parameter optimized

in this study to increase the stability of ilmenite solution for ternary MgO-MnO-TiO_2 system (see Table 2).

4.4 Cubic Spinel, Tetragonal Spinel, Monoxide and Rutile Solid Solution

Apart from the above-mentioned phases, several solid solutions having distinctive crystal structures and solubility limits are observed in the MgO-MnO-Mn_2O_3-Ti_2O_3-TiO_2 system, as listed in Table 1. Cubic and tetragonal spinels were modeled separately due to different crystal structure and availability of information on phase transformation.[16–18,40] Two-sublattice model in the framework of the Compound Energy Formalism (CEF)[33] was used to describe both the spinel phases. Mg^{2+}, Mn^{2+}, Mn^{3+}, Mn^{4+}, Ti^{3+} and Ti^{4+} cations are present in two cationic sublattices in spinel: tetrahedral site (T) and octahedral site (O). Vacancy was also introduced in the octahedral site to model non-stoichiometry toward oxygen-rich composition.

The monoxide solid solution is the solid solution based on MO oxides where M^{2+} is a divalent cation such as Mg^{2+}, Ca^{2+}, Fe^{2+}, Mn^{2+}, Co^{2+}, Ni^{2+}, etc.[41] It is often called as halite (rock salt) solution for its structural similarity with NaCl crystal (halite). Rutile has a body-centered tetragonal structure which has non-stoichiometry toward the Ti_2O_3 direction and is usually expressed as $TiO_{2-\delta}$.[18] As the defect mechanism is not clear, all divalent, trivalent, and tetravalent cations are assumed to mix randomly on the cationic sublattice. Both monoxide and rutile solution were modeled using the Bragg-Williams random mixing model[29] and the results from the previous studies[16–18] were used without any modification.

4.5 Stochiometric, Metallic and Gas Phases

In this study, the Gibbs energies of Magnéli phases (Ti_nO_{2n-1}, $n \geq 4$), Mg_6MnO_8 and other stoichiometric oxides (MnO_{2-}, α-Mn_2O_3, β-Mn_2O_3) were taken from previous studies[16,40,42] (now stored in FACT pure substance database) and the Gibbs energies of all metallic phases and gasses species were taken from the FACT pure substance database.[15]

5 Experimental Results

The purpose of the present experimental phase diagram study was to determine the liquidus and sub-solidus phase equilibria in the ternary Mg-Mn-Ti-O system in air. The results of phase diagrams experiments are summarized in Table 3. The BSE images and XRD patterns of several equilibrated samples are presented in Fig. 2 and 3, respectively. The equilibration time was long enough (12-70 h) to bring the samples to equilibration before getting quenched in ice-cold water. For lower temperature, long equilibration hours were chosen. The small standard deviation ($2\sigma \leq 0.01$) in the composition of each solid phase in Table 3 indicates the samples were very well equilibrated. For liquid phase, exsolution behavior has been seen which could lead to a large standard deviation in the equilibrium composition. Therefore, area analysis (20 μm × 20 μm or/and 10 μm × 10 μm) was performed for liquid (glass) phase, and spot analysis of 1 to 3 μm in diameter was performed for solid phases. No Mg, Mn and Ti solubility was found in Pt crucible and no Pt was detected in oxide phases. EPMA cannot distinguish different oxidation states of metals, so the experimental composition results are only summarized as Mg, Mn and Ti metallic composition in Table 3.

As can be seen in the microstructures in Fig. 2(a), (b), (c), and (d), the equilibrium solid phases (pseudobrookite, ilmenite, spinel, rutile) were very well developed in each sample. Exsolutions are seen in liquid phase. Samples MMT7 was quenched to single glass, which shows no shift in the composition from the original starting composition. This confirms the accuracy of composition analysis for liquid phase. Six samples (MMT 3, 5, 6,10-12) at different temperatures forms two phase equilibria of 'pseudobrookite + ilmenite' (For example, see Fig. 2b for MMT3). It should be noted that the composition of MMT3 was originally designed for ilmenite single phase region, but very small amount pseudobrookite phase was also seen possible due to slight deviation of original composition. XRD analysis of MMT5 (see Fig. 3b) also confirms the presence of these two solid solutions: ilmenite (PDF: 04-076-3017, SG: $R\bar{3}$) and pseudobrookite (PDF: 01–086–0148, SG: Bbmm). Three phase equilibria of 'liquid + pseudobrookite + spinel' at 1450 °C (MMT1) and 'liquid + pseudobrookite + rutile' at 1500 °C (MMT4) can be clearly seen in Fig. 2(a) and (c), respectively. XRD analysis of MMT4 (see Fig. 3a) confirms the glass peak along with the pseudobrookite and rutile phase (PDF: 04–014–8907, SG: $P4_2/mnm$). MMT 8 and 9 at 1550 °C show two phase equilibria of 'liquid + pseudobrookite' and 'liquid + rutile', respectively. No evidence of any ternary stoichiometric compound was found within the temperature and composition ranges investigated.

Within the Mg-Mn-Ti-O system in air, a large amount of manganese is still present as Mn^{2+} rather than Mn^{3+}, while all titanium could be assumed in Ti^{4+} state. As Mn^{2+}/Mn^{3+} ratios in the equilibrated samples are not known, the proper way to present experimental data is to compare the experimental data with the calculated phase diagram of the MgO-MnO-TiO_2 in air, as shown in Fig. 4.

Table 3 Equilibrium experimental results for the Mg-Mn-Ti-O system in air

Sample	Starting composition			Temperature	Time	Phases(a) (#)	Phase composition, mole fraction		
	TiO_2	MgO	MnO	C	Hours		Ti	Mg	Mn
MMT1	0.50	0.20	0.30	1450	12	Liq (11)	0.496 ± 0.008	0.128 ± 0.006	0.376 ± 0.010
						Psb (22)	0.647 ± 0.005	0.215 ± 0.006	0.138 ± 0.005
						Spi (10)	0.318 ± 0.008	0.294 ± 0.007	0.388 ± 0.010
MMT2	0.50	0.20	0.30	1500	12	Liq (4)	0.493 ± 0.017	0.112 ± 0.029	0.395 ± 0.046
						Ilm (15)	0.508 ± 0.004	0.246 ± 0.003	0.246 ± 0.003
MMT3	0.50	0.20	0.30	1400	24	Psb (10)	0.645 ± 0.003	0.212 ± 0.004	0.143 ± 0.002
						Ilm (10)	0.502 ± 0.006	0.204 ± 0.007	0.294 ± 0.008
MMT4	0.70	0.10	0.20	1500	24	Liq (24)	0.647 ± 0.015	0.045 ± 0.025	0.308 ± 0.030
						Psb (14)	0.669 ± 0.005	0.207 ± 0.007	0.124 ± 0.004
						Rut (9)	0.996 ± 0.001	0.001 ± 0.001	0.003 ± 0.001
MMT5	0.60	0.30	0.10	1400	24	Psb (17)	0.657 ± 0.007	0.268 ± 0.009	0.075 ± 0.003
						Ilm (5)	0.505 ± 0.001	0.332 ± 0.015	0.163 ± 0.007
MMT6	0.60	0.30	0.10	1450	24	Psb (43)	0.652 ± 0.006	0.278 ± 0.006	0.07 ± 0.006
						Ilm (7)	0.499 ± 0.006	0.345 ± 0.012	0.156 ± 0.012
MMT7	0.50	0.20	0.30	1550	40	Liq (27)	0.500 ± 0.009	0.203 ± 0.010	0.297 ± 0.009
MMT8	0.60	0.30	0.10	1550	40	Liq (16)	0.502 ± 0.008	0.260 ± 0.056	0.255 ± 0.057
						Psb (11)	0.659 ± 0.009	0.283 ± 0.012	0.058 ± 0.003
MMT9	0.70	0.10	0.20	1550	40	Liq (17)	0.678 ± 0.026	0.153 ± 0.044	0.169 ± 0.041
						Rut (5)	0.997 ± 0.001	0.001 ± 0.001	0.002 ± 0.001
MMT10	0.60	0.30	0.10	1500	24	Psb (31)	0.659 ± 0.006	0.271 ± 0.007	0.070 ± 0.002
						Ilm (9)	0.505 ± 0.005	0.344 ± 0.007	0.151 ± 0.005
MMT11	0.50	0.20	0.30	1250	70	Psb (6)	0.642 ± 0.009	0.225 ± 0.008	0.134 ± 0.002
						Ilm (24)	0.497 ± 0.004	0.210 ± 0.004	0.293 ± 0.004
MMT12	0.60	0.30	0.10	1250	70	Psb (11)	0.646 ± 0.003	0.284 ± 0.008	0.070 ± 0.007
						Ilm (3)	0.497 ± 0.007	0.355 ± 0.010	0.148 ± 0.007

(a) Liq = Liquid, Psb = Pseudobrookite, Spi = Cubic spinel, Ilm = Ilmenite, and Rut = Rutile

#means the number of analysis for each phase

6 Critical Evaluation and Optimizations

New phase diagram experimental data from this current study and experimental data available from the literature[19] were simultaneously considered to obtain a set of Gibbs energy functions for all the phases in this quinary MgO-MnO-Mn_2O_3-Ti_2O_3-TiO_2 system.

Predicted phase diagrams of the MgO-MnO-Ti_2O_3 in Mn saturation and MgO-MnO-TiO_2 in air are calculated at 1000 °C and presented in Fig. 5. Monoxide, spinel and ilmenite solutions are stable under reducing atmosphere (Mn saturation), and all the solution phases are stable in air. Because Ti has Ti^{3+} and Ti^{4+} in reducing condition (Mn saturation), and Mn is only in Mn^{2+} state, the spinel phase is stable along the $MnTi_2O_4$-$MgTi_2O_4$. Ti_2O_3-rich ilmenite solution, and MgO-MnO monoxide solution are also well developed under the reducing atmosphere. However, under oxidizing condition (air), Mn has both Mn^{2+} and Mn^{3+}states and Ti is only in Ti^{4+} state. As results, Mn^{3+} containing cubic and tetragonal spinel solutions compassing Mg_2TiO_4-$MgTi_2O_4$-$MgMn_2O_4$-$MnTi_2O_4$-Mn_3O_4-Mn_2TiO_4 are developed. In addition, ilmenite solution of $MgTiO_3$-$MnTiO_3$, and pseudobrookite solution of $MgTi_2O_5$ dissolving excess Mn oxide ($MnTi_2O_5$) are also formed.

The isothermal phase diagrams of the Mg-Mn-Ti-O system in air are calculated in Fig. 6 from the present thermodynamic models with optimized parameters. Pseudobrookite and ilmenite solutions show line solid solutions while stability areas of cubic spinel, tetragonal spinel and liquid solutions are changed significantly depending on temperature. The new phase diagram experimental data in this study are compared with the calculated phase diagrams, which shows reasonable agreement at all temperatures. The experimental data of Demin et al.[19] at 1100 and 1200 °C (see Fig. 6a and b), except the stability of tetragonal spinel phase at 1200 °C, are well reproduced in

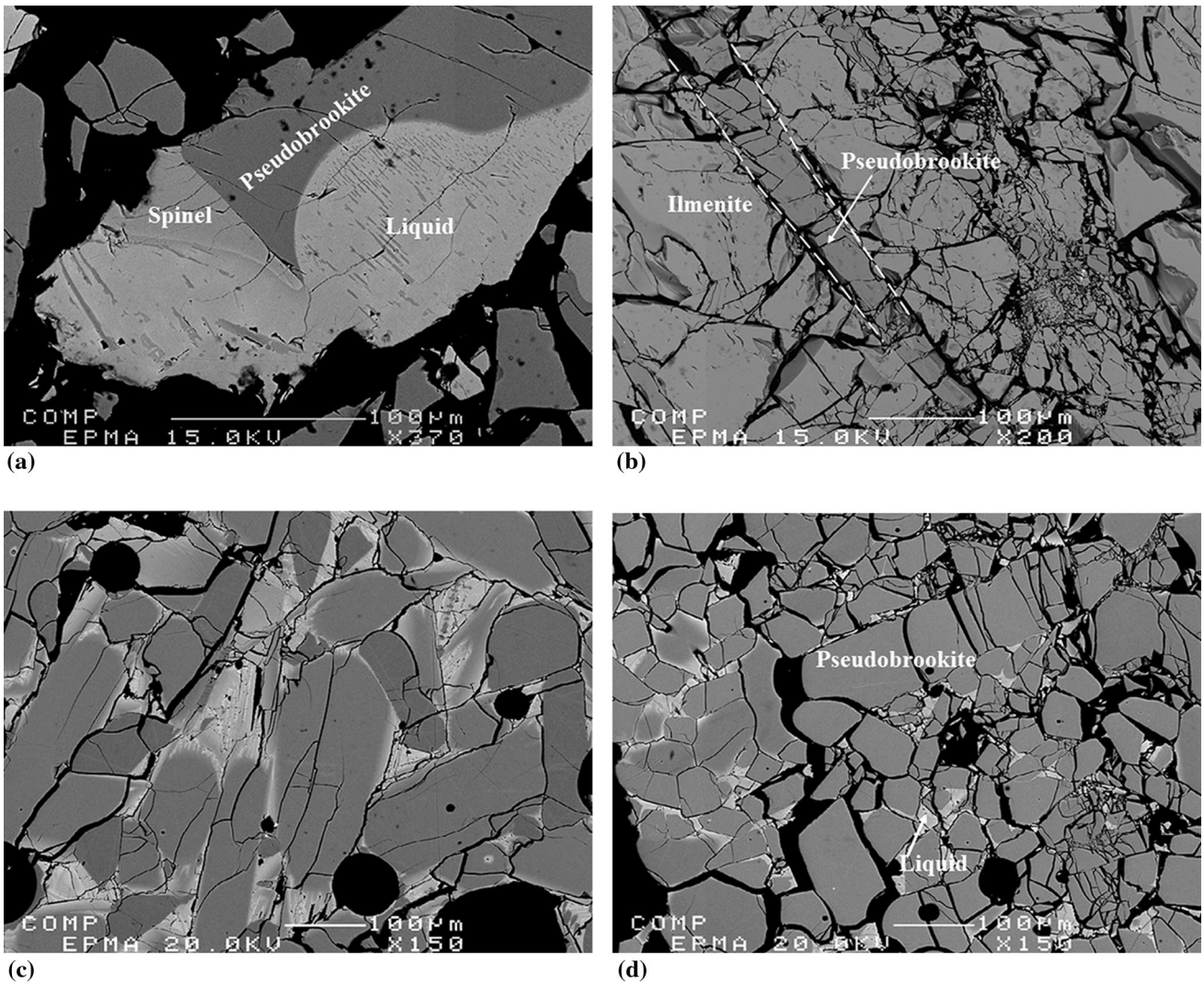

Fig. 2 Backscattered electron images (BSE) of the equilibrated samples. (a) MMT1, (b) MMT3, (c) MMT4, and (d) MMT8

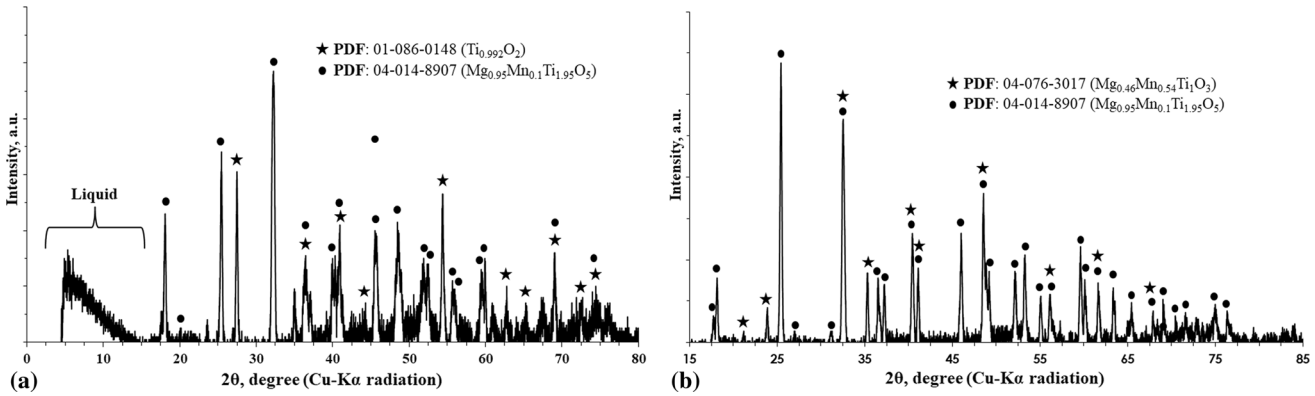

Fig. 3 XRD patterns of equilibrated quenched samples. (a) MMT4, and (b) MMT5

this study. Kang and Jung[40] reviewed the experimental data of pure Mn_3O_4 and reported that tetragonal spinel transforms to cubic spinel at about 1175 °C in air. In addition, for the Mg-Mn-O[17] and Mn-Ti-O[18] systems, it is already known that the transition temperature of Mn_3O_4 tetragonal spinel to cubic spinel solution decreases with

increasing the solubility of Mg and Ti oxides in spinel solution. Therefore, this disagreement about tetragonal spinel phase in Fig. 6(b) happens most probably due to the fast transformation of equilibrium cubic spinel phase (MnO mol.% $\geq$ 60) to tetragonal distorted cubic spinel (tetragonal spinel) in the quenching process by Demin et al.[19] A positive excess parameter for tetragonal spinel was introduced to reproduce its stability area at 1100 °C, as shown in Fig. 6(a).

As the stability of different solid solutions are sensitive to temperature, which we can see clearly from the optimization results in Fig. 6, formation of low temperature phases during quenching was inevitable. Therefore, quenched phase formation was a big issue in the current investigation. At 1250, 1400 and 1450 °C, the two phase pseudobrookite and ilmenite formation is well reproduced from current thermodynamic optimization. The tie-line calculations are also performed at starting composition which are in good agreement with the experimental data. At 1450 °C, three phase equilibria were found at one of the equilibrated compositions which seem to lie exactly at the four-phase boundary of the cubic spinel, pseudobrookite, ilmenite and liquid phase stability (see Fig. 6e). And, slight deviation in the sampling composition or equilibration temperature can lead to formation of any two to three-phase combinations. And, overall quenching issue, there is good possibility of transition of some section of sample from one phase to another. A negative excess parameter for cubic spinel was used to reproduce the three phase equilibria at 1450 °C, as shown in Fig. 6(e). Due to low viscous slag, exsolution effects occurred from the slag phase during quenching at 1500 and 1550 °C, which leads to large error range in the EPMA analysis, as shown in Fig. 2(c) and (d) and displayed in Fig. 6(f) and (g). At 1500 °C, the three-phase stability between liquid, pseudobrookite and rutile are well reproduced within experimental error range. The ilmenite + pseudobrookite and liquid + ilmenite phase formation at 1500 °C was difficult to reproduce which might be due to bad quenching or exsolution of ilmenite phase at low temperature. MMT10 at 1500C was believed to be initially Psb + CSpi, but, due to quenching issue, the ilmenite phase got formed at low temperatures which got stable at the equilibrated samples. Initially, MMT2 is believed to be liquid phase at 1500 °C as shown

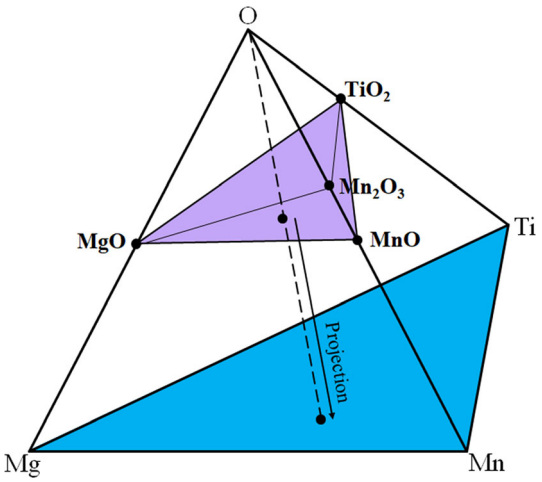

Fig. 4 Graphic representation of experimental data in MgO-MnO-Mn_2O_3-TiO_2 system from oxygen corner

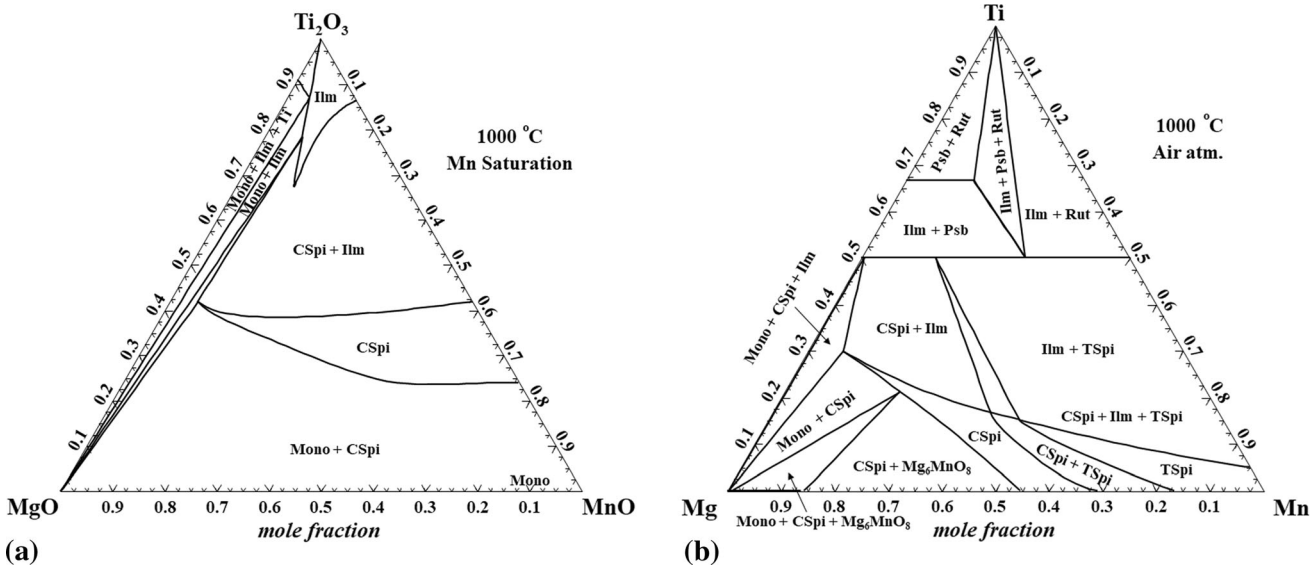

Fig. 5 Predicted phase diagram of Mg-Mn-Ti-O system at 1000 °C. (a) Phase diagram of the MgO-MnO-Ti_2O_3 in Mn saturation, and (b) MgO-MnO-TiO_2 in air condition. See Table 1 for abbreviation of phase names

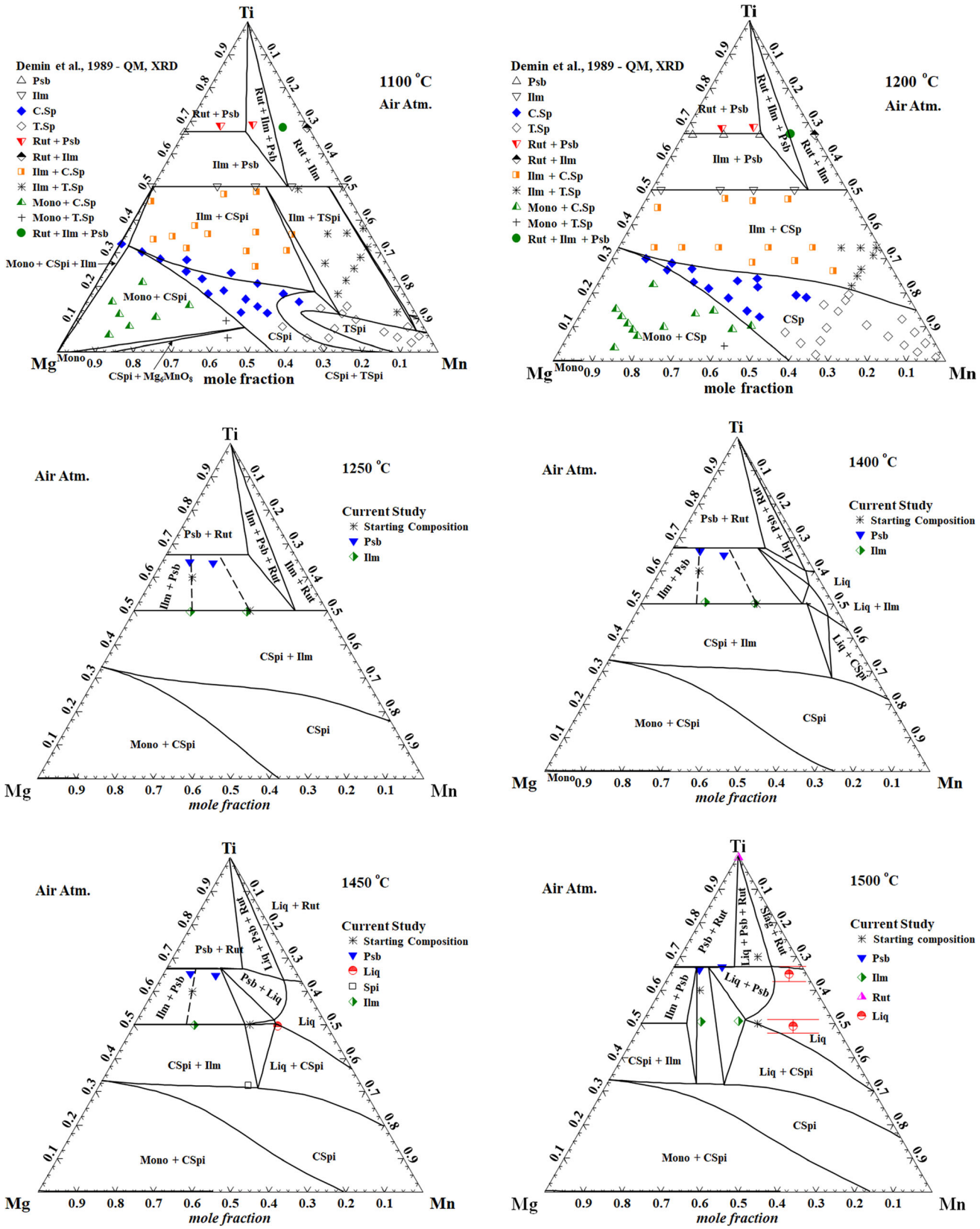

Fig. 6 Calculated phase diagrams of the MgO-MnO-TiO_2 in air along with the experimental data by Demin et al.[19] and in the present study

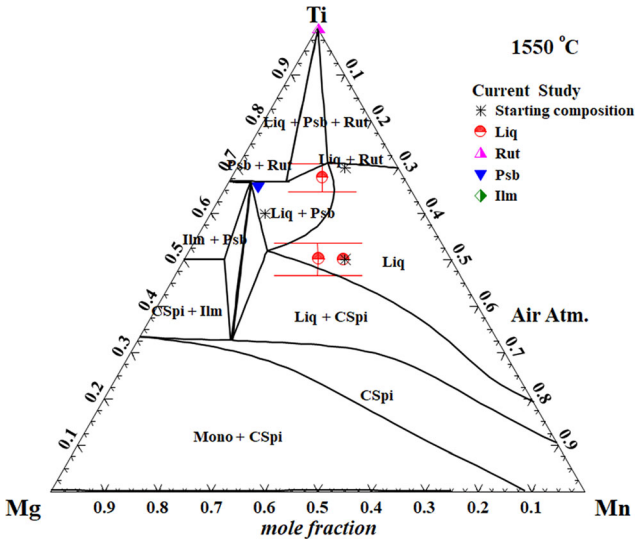

Fig. 6 continued

in the Fig. 6(f). But, due to quenching issue, ilmenite phases in the samples got stable (the solid solution closest to the sampling composition) at low temperature. Therefore, the liquid composition also goes towards right (lower Mg-side). At 1550 °C, the phase equilibria are in good agreement with the current modeling within the experimental error limit. For solid phase, the standard deviation (2σ) was found to be less than 0.01. Unfortunately, there are no reliable experimental phase diagram data in this quaternary system at reducing condition for comparison.

Figure 7 shows the predicted phase diagram of MgO-MnO-Ti_2O_3 system in Mn saturation at 1500 °C and 1900 °C. The parameters of solid solutions are fixed already in order to reproduce the phase diagrams in air condition (explained earlier). As, no phase diagram data are present for the reduced condition (or Mn saturation), the liquid region was fixed from using ternary interpolation from binary parameters. Above 1500 °C, the liquid phase starts forming from MnO-Ti_2O_3 side. With increasing temperature, cubic spinel (CSpi) and ilmenite (Ilm) phase get destabilized from MnO-Ti_2O_3, as shown in Fig. 7(b). Phase equilibrium experiments needs to be performed for this system at reduced condition in order to confirm the current prediction shown in Fig. 7.

The calculated liquidus projections of the Mg-Mn-Ti-O system in Mn saturation and in air condition are presented in Fig. 8. No ternary stochiometric compound was assumed. The thin lines and thick lines represent the isotherms and invariant lines, respectively, and primary crystalline phases are indicated. Cubic spinel solution is very stable in both reducing and oxidizing conditions. While ilmenite, monoxide and cubic spinels are crystallized as primary solid phases in reducing condition, additional rutile and pseudobrookite phases are formed in air. The predicted invariant reactions involving liquid phase in air are summarized in Table 4.

The predicted isopleth of the Mg_2TiO_4-Mn_2TiO_4 in air atmosphere is presented in Fig. 9(a). The relative amount of cubic spinel and ilmenite at subsolidus temperatures (for example, 1200 °C) can be varied with composition; the amount of ilmenite increases with increasing Mn_2TiO_4. Figure 9(b) shows the predicted cation distribution in Mg_2TiO_4-Mn_2TiO_4 spinel solution at 1200 and 1400 °C. In the calculations, we assumed only spinel solution by suppressing the formation of ilmenite solution. There is no difference in Ti^{4+} cations in octahedral site for 1200 and 1400 °C, but the competition of Mg^{2+} and Mn^{2+} in octahedral and tetrahedral sites can be found depending on the composition. For example, at equimolar composition of Mg_2TiO_4 and Mn_2TiO_4, Mg^{2+} and Mn^{2+} cations have tendency to occupy tetrahedral and octahedral sites, respectively.

7 Summary

Thermodynamic optimization of the MgO-MnO-Mn_2O_3-TiO_2-Ti_2O_3 system at a total pressure of 1 atm has been carried out. Due to lack of phase equilibrium data in oxidizing atmosphere, phase diagram experiments on the Mg-Mn-Ti-O system in air were carried out, followed by the phase characterization using the XRD and EPMA. The stability of solid solutions is so sensitive at high temperature, it was very difficult to get a good quenched sample. The thermodynamic models with optimized parameters reproduced all the reliable experimental data within experimental error limits and were used to predict unknown phase diagrams and structural cation distribution data in spinel solution. However, more experimental studies need to be performed for better understanding of stability of solid and liquid solutions. The present database containing optimized parameters along with general thermodynamic software, such as FactSage, can calculate phase equilibria, thermodynamic properties and structural data of the MgO-MnO-Mn_2O_3-TiO_2-Ti_2O_3 system at any given set of conditions under 1 atm total pressure.

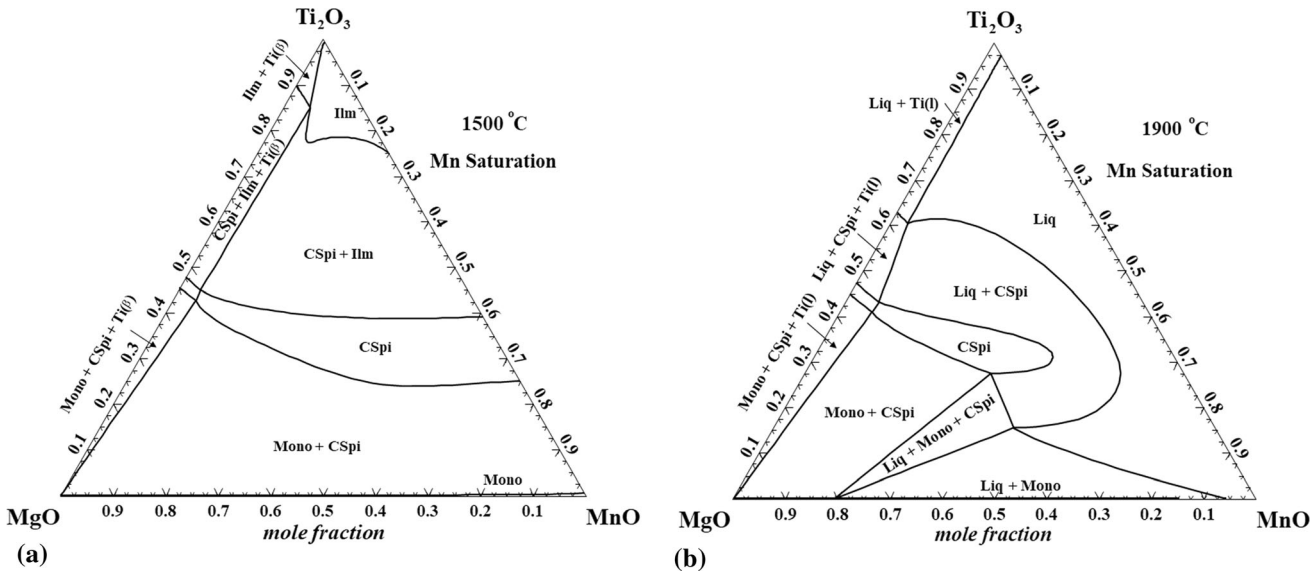

Fig. 7 Predicted phase diagrams of MgO-MnO-Ti_2O_3 system in Mn saturation, (a) 1600 °C, and (b) 1800 °C

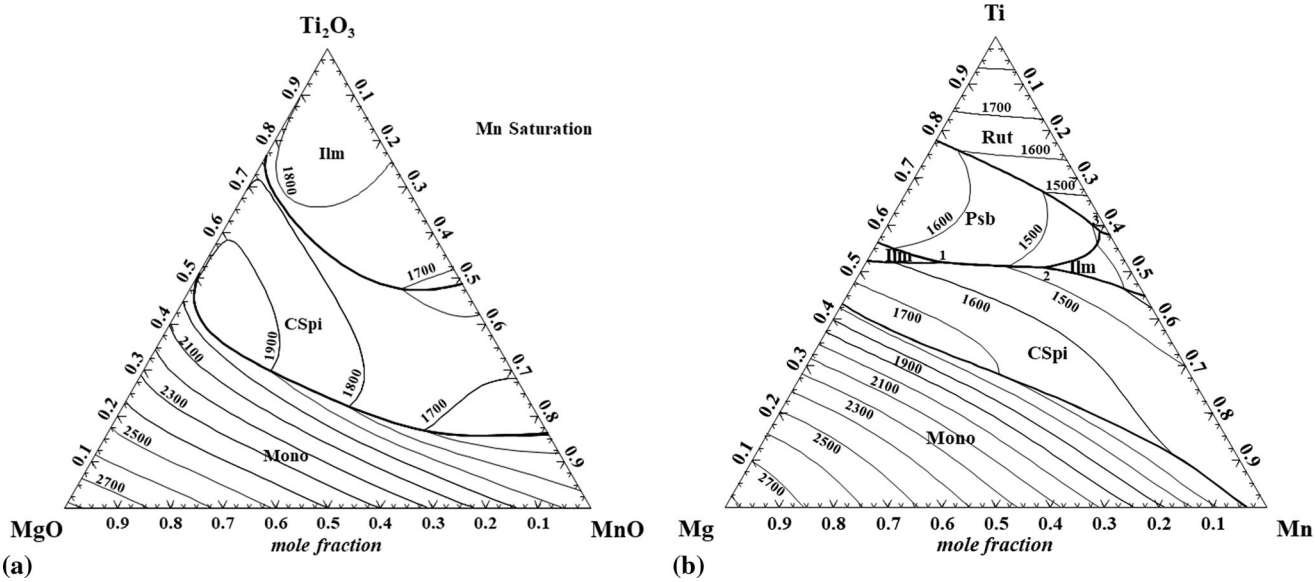

Fig. 8 Predicted liquidus projection of the Mg–Mn-Ti–O system. (a) Mn saturation, and (b) air

Table 4 Invariant reactions involving liquid phase in the Mg–Mn-Ti–O system in air atmosphere, predicted from the present optimization

No.(a)	Phases in equilibrium with liquid	Composition (mole fraction)			Temp., °C
		Ti	Mg	Mn	
1	CSp + Ilm + Psb	0.52	0.39	0.14	1551
2	CSp + Ilm + Psb	0.51	0.16	0.33	1463
3	Ilm + Psb + Rut	0.59	0.01	0.40	1379

(a) The number indexs of the invariant reactions are the same as the ones in Fig. 8(b)

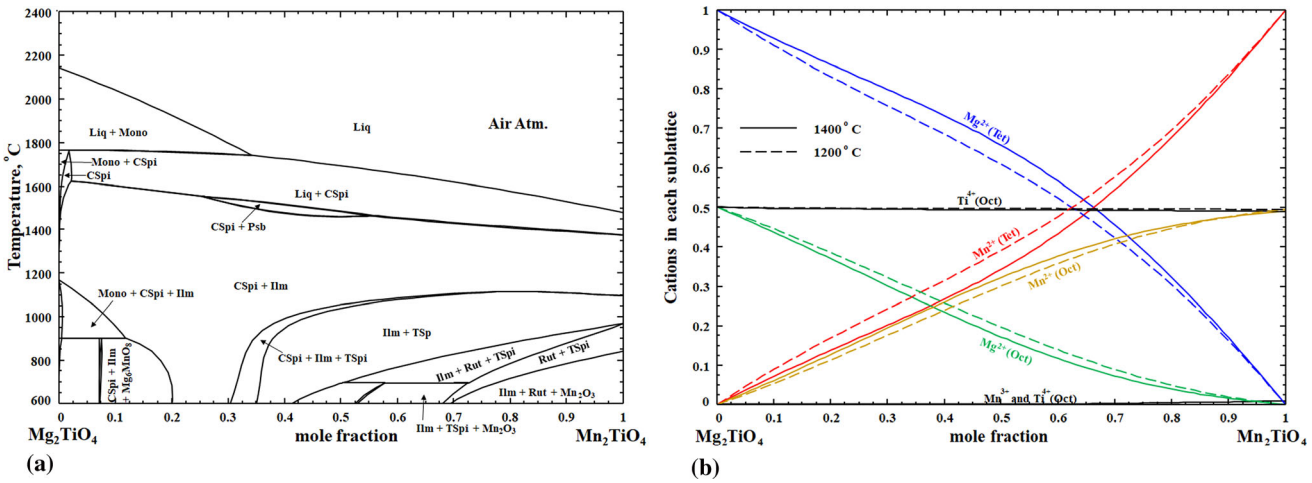

Fig. 9 (a) Calculated isopleth of the Mg_2TiO_4-Mn_2TiO_4 in air, and (b) cation distribution in the cubic spinel Mg_2TiO_4-Mn_2TiO_4 solution at 1200 °C and 1400 °C

Acknowledgments Financial support from Hyundai Steel, JFE Steel, Nippon Steel and Sumitomo Metals Corp., Nucor Steel, POSCO, RHI, RioTinto Iron and Titanium, RIST, Schott A.G., Tata Steel Europe, Voestalpine Stahl, and the Natural Sciences and Engineering Research Council of Canada are gratefully acknowledged. This work was also supported by the National Research Foundation of Korea (NRF) grant funded by the Korea government (MSIT) (No. NRF-2015R1A5A1037627). One of the authors (S.K. Panda) would like to thank the McGill Engineering Doctorate Award (MEDA) program.

References

1. T. Tsunooka, M. Androu, Y. Higashida, H. Sugiura, and H. Ohsatoc, Effects of TiO_2 on Sinterability and Dielectric Properties of High-Q Forsterite Ceramics, *J. Eur. Ceram. Soc.*, 2013, **23**, p 2573-2578
2. A. Belous, O. Ovchar, D. Durilin, M. Krzmanc, M. Valant, and D. Suvorov, High-Q Microwave Dielectric Materials Based on the Spinel Mg_2TiO_4, *J. Am. Ceram. Soc.*, 2006, **89**, p 3441-3445
3. J.C. Kim, M.-H. Kim, J.-B. Lim, S. Nahmw, J.-H. Paik, and J.-H. Kim, Synthesis and Microwave Dielectric Properties of $Re_3Ga_5O_{12}$ (Re: Nd, Sm, Eu, Dy, Yb, and Y) Ceramics, *J. Am. Ceram. Soc.*, 2007, **90**, p 641-644
4. W. Lei, W.-Z. Lu, J.-H. Zhu, F. Liang, and D. Liu, Modification of $ZnAl_2O_4$-Based Low-Permittivity Microwave Dielectric Ceramics by Adding 2MO–TiO_2 (M = Co, Mg, and Mn), *J. Am. Ceram. Soc.*, 2008, **91**, p 1958-1961
5. P.S. Anjana and M.T. Sebastian, Synthesis, Characterization, and Microwave Dielectric Properties of $ATiO_3$ (A = Co, Mn, Ni) Ceramics, *J. Am. Ceram. Soc.*, 2006, **89**, p 2114-2117
6. T. Hamieh, F. Kawtharani, A. Kassas, R. Quercioli, D. Houivet, J. Bernard, H. Lakiss, J. Toufaily, R. Aoun, and M. Reda, Ultrafine Grinding of $MgTiO_3$ Based Ceramic Influencing the Material Properties, *J Phys. Chem. Biophys.*, 2013, **3**, p 122-134
7. I. Lorite, M.A. Rodriguez, F. Azough, R. Freer, and J.F. Fernandez, $ZnAl_2O_4$ and (0.79) $ZnAl_2O_4$–(0.21)Mn_2TiO_4 Microwave Dielectric Ceramics Prepared by Hot Pressing and Spark Plasma Sintering, *J. Am. Ceram. Soc.*, 2012, **95**, p 1023-1028
8. T. Li, C. Wang, X. Sun, G. Wang, C. Lei, and L. Liu, Surface-Layer Effect in $MnTiO_3$ Ceramics at Low Temperatures, *Phys. B*, 2012, **407**, p 4749-4751
9. I.-H. Jung, S.A. Decterov, and A.D. Pelton, Computer Applications of Thermodynamic Databases to Inclusion Engineering, *ISIJ Int.*, 2004, **44**, p 527-536
10. J. Takamura, S. Mizoguchi, Roles of oxides in steels performance—Metallurgy of oxides in steels, in Proc. 6th Int. Iron and Steel Cong, Tokyo, ISIJ, vol. 1 (1990), pp. 591–597
11. I.-H. Jung, Y.-B. Kang, S.A. Decterov, and A.D. Pelton, Thermodynamic Evaluation and Optimization of the MnO-Al_2O_3 and MnO-Al_2O_3-SiO_2 Systems and Applications to Inclusion Engineering, *Met. Mat. Trans. B*, 2004, **35**, p 259-268
12. Y.-B. Kang, H.S. Kim, J. Zhang, and H.-G. Lee, Practical Application of Thermodynamics to Inclusions Engineering in Steel, *J. Phys. Chem. Solids*, 2005, **66**, p 219-225
13. C.-H. Chang, I.-H. Jung, S.-C. Park, H.S. Kim, and H.-G. Lee, Effect of Mg on the Evolution of Non-metallic Inclusions in Mn-Si-Ti Deoxidized Steel During Solidification: Experiments and Thermodynamic Calculations, *Ironmak. Steelmak.*, 2005, **32**, p 251-257
14. S.-C. Park, I.-H. Jung, K.-S. Oh, and H.-G. Lee, Effect of Al on the Evolution of Non-metallic Inclusions in the Mn–Si–Ti–Mg Deoxidized Steel During Solidification: Experiments and Thermodynamic Calculations, *ISIJ Int.*, 2004, **44**, p 1016-1023
15. C.W. Bale, E. Bélisle, P. Chartrand, S.A. Decterov, G. Eriksson, A.E. Gheribi, K. Hack, I.-H. Jung, Y.-B. Kang, J. Melançon, A.D. Pelton, S. Petersen, C. Robelin, J. Sangster, P. Spencer, and M.-A. Van Ende, FactSage Thermochemical Software and Databases, *Calphad*, 2016, **54**, p 35-53
16. S.K. Panda and I.-H. Jung, Critical Evaluation and Thermodynamic Modeling of the Mg-Mn-O (MgO-MnO-MnO_2) System, *J. Am. Ceram. Soc.*, 2014, **97**, p 3328-3340
17. X. Du, I.-H. Jung, Thermodynamic Modeling of the MgO-Ti_2O_3-TiO_2 System, Metall. Mater. Trans. B (2018), to be submitted
18. S.K. Panda, P. Hudon, I.-H. Jung, Coupled Experimental Study and Thermodynamic Modeling of the MnO-Mn_2O_3-Ti_2O_3-TiO_2 system, *Calphad*, 2019, **66**. https://doi.org/10.1016/j.calphad.2019.101639
19. V.P. Demin, A.M. Yankin, and V.F. Balakirev, Phase Diagrams of the System Magnesium-Mangnaese-Titanium-Oxygen in Open Air at 1100 °C and 1200 °C, *Inorg. Mater.*, 1989, **25**, p 840-843
20. Y.-B. Kang and I.-H. Jung, Critical Evaluations and Thermodynamic Optimizations of the MnO-Mn_2O_3-SiO_2 and FeO-Fe_2O_3-MnO-Mn_2O_3-SiO_2 Systems, *Met. Mat. Trans. B*, 2017, **48**, p 1721-1735

21. S.K. Panda, Z. Cao, and I.-H. Jung, Critical Evaluation and Thermodynamic Modeling of the MgO–MnO–Mn_2O_3–SiO_2 System, *J. Am. Ceram. Soc.*, 2015, **98**, p 2921-2930
22. S.K. Panda, I.-H. Jung, Coupled Experimental Study and Thermodynamic Modeling of the Al_2O_3-Ti_2O_3-TiO_2 System, *ISIJ Int.*, 2020, **60**, p 31–41.
23. S.K. Panda, I.-H. Jung, Coupled Experimental Study and Thermodynamic Modeling of the FeO-Fe_2O_3-Ti_2O_3-TiO_2 System, Geochim. Cosmochim. Acta (2018), to be submitted
24. A. Navrotsky, Thermodynamics of Formation of Some Compounds with the Pseudobrookite Structure and of the $FeTi_2O_5$-Ti_3O_5 Solid Solution Series, *Am. Mineral.*, 1975, **60**, p 249-256
25. A.D. Pelton, M. Blander, Computer-assisted analysis of the thermodynamic properties and phase diagrams of slags, in Proc. 2nd Int. Symp. on Metall. Slags and Fluxes, TMS-AIME, Warrendale, Pennsylvania (1984), pp. 281–294
26. A.D. Pelton and M. Blander, Thermodynamic Analysis of Ordered Liquid Solutions by a Modified Quasichemical Approach—Application to Silicate Slags, *Metall. Mater. Trans. B*, 1986, **17**, p 805-815
27. A.D. Pelton, S.A. Degterov, G. Eriksson, C. Robelin, and Y. Dessureault, The Modified Quasichemical Model. I. Binary Solutions, *Metall. Mater. Trans. B*, 2000, **31**, p 651-659
28. A.D. Pelton and P. Chartrand, The Modified Quasichemical Model. II. Multicomponent Solutions, *Metall. Mater. Trans. A*, 2001, **32**, p 1355-1360
29. A.D. Pelton, A General "Geometric" Thermodynamic Model for Multicomponent Solutions, *Calphad*, 2001, **25**, p 319-328
30. W.Q. Guo, S. Malus, D.H. Ryan, and Z. Altounian, Crystal Structure and Cation Distributions in the $FeTi_2O_5$-Fe_2TiO_5 Solid Solution Series, *J. Phys.: Condens. Matter*, 1999, **11**, p 6337-6346
31. A.R. Lennie, K.S. Knight, and C.M.B. Henderson, Cation Ordering in $MgTi_2O_5$ (karrooite); Probing Temperature Dependent Effects of Neutrons, *Am. Mineral.*, 2007, **92**, p 1165-1180
32. G. Seitz, N. Penin, L. Decoux, A. Wattiaux, M. Duttine, and M. Gaudon, Near the Ferric Pseudobrookite Composition (Fe_2TiO_5), *Inorg. Chem.*, 2016, **55**, p 2499-2507
33. M. Hillert, B. Jansson, and B. Sundman, Application of the Compound-Energy Model to Oxide Systems, *Z. Metallkd.*, 1988, **79**, p 81-87
34. R.H. Mitchell and R.P. Liferovich, The Pyrophanite–Ecandrewsite Solid-Solution Series: Crystal Strucutres of the Mn1-xZnxTiO3 Series ($0.1 \leq x \leq 0.8$), *Can. Metal.*, 2004, **42**, p 1871-1880
35. R.P. Liferovich and R.H. Mitchell, The Pyrophanite–Geikielite Solid-Solution Series: Crystal Strucutres of the Mn1-xMgxTiO3 Series ($0 < x < 0.7$), *Can. Metal.*, 2006, **44**, p 1099-1107
36. R.P. Liferovich and R.H. Mitchell, Mn, Mg, and Zn Ilmenite Group Titanates: a Reconnaissance Rietveld Study, *Crystallogr. Rep.*, 2006, **51**, p 383-390
37. X. Wu, S. Qin, and L. Dubrovinsky, Structural Characterization of the $FeTiO_3$–$MnTiO_3$ Solid Solution, *J. Solid State Chem*, 2010, **183**, p 2483-2490
38. R.J. Harrison, U. Becker, and S.A.T. Redfern, Thermodynamics of the $R\bar{3}$ to $R\bar{3}c$ Phase Transition in the Ilmenite-Hematite Solid Solution, *Am. Miner.*, 2000, **85**, p 1694-1705
39. R.J. Harrison, S.A.T. Redfern, and R.I. Smith, In-situ Study of the $R\bar{3}$ to $R\bar{3}c$ Phase Transition in the Ilmenite-Hematite Solid Solution Using Time-of-Flight Neutron Powder Diffraction, *Am. Mineral.*, 2000, **85**, p 194-205
40. Y.-B. Kang and I.-H. Jung, Thermodynamic Modeling of Oxide Phases in the Mn-O System, *J. Phys. Chem. Solids*, 2016, **98**, p 237-246
41. I.-H. Jung, Critical Evaluation and Thermodynamic Modeling of Phase Equilibria in Multicomponent Oxide Systems. PhD Thesis, École Polytechnique, Montréal, 2003, p 338
42. Y.-B. Kang, I.-H. Jung, and H.-G. Lee, Critical Thermodynamic Evaluation and Optimization of the MnO-"TiO_2"-"Ti_2O_3" System, *Calphad*, 2006, **30**, p 235-247
43. G. Eriksson and A.D. Pelton, Critical Evaluation and Optimization of the Thermodynamic Properties and Phase Diagrams of the MnO-TiO_2, MgO-TiO_2, FeO-TiO_2, Ti_2O_3-TiO_2, Na_2O-TiO_2, and K_2O-TiO_2 Systems, *Mater. Trans. B*, 1993, **24**, p 795-805
44. G. Eriksson and A.D. Pelton, Critical Evaluation and Optimization of the Thermodynamic Properties and Phase Diagrams of the CaO-Al_2O_3, Al_2O_3-SiO_2, and CaO-Al_2O_3-SiO_2 Systems, *Mater. Trans. B*, 1993, **24**, p 807-816